

Adaptive optics enhanced simultaneous *en-face* optical coherence tomography and scanning laser ophthalmoscopy

David Merino and Chris Dainty

Applied Optics Group, Department of Experimental Physics,
National University of Ireland, Galway, Ireland

david.merino@nuigalway.ie

c.dainty@nuigalway.ie

Adrian Bradu and Adrian Gh. Podoleanu

Applied Optics Group, School of Physical Sciences,
University of Kent at Canterbury, CT2 7NR, UK

a.bradu@kent.ac.uk

a.g.h.podoleanu@kent.ac.uk

Abstract: A novel combination of adaptive optics with a simultaneous *en-face* OCT/SLO system for high resolution imaging of the *in-vivo* human retina is presented. Pairs of retinal images are shown and performance of the system is evaluated with and without dynamic wavefront correction. The adaptive optics closed loop system operates at a frame rate of 9 Hz and incorporates a Shack-Hartmann wavefront sensor based on a highly sensitive Andor camera and a 37 actuator OKO membrane deformable mirror to correct for ocular aberrations. The system produces C-scan pairs of images at a frame rate of 2 Hz. The correction of aberrations produced by the adaptive optics closed-loop system increased the signal-to-noise ratio in images obtained from volunteer eyes by up to 6 dB in the OCT channel and up to 9 dB in the SLO channel. A slight improvement in the lateral resolution was also obtained, from 6.5 μm before to 5 μm after closing the adaptive optics loop.

© 2006 Optical Society of America

OCIS codes: (010.1080) Adaptive Optics; (170.4500) Optical Coherence Tomography; (170.4460) Ophthalmic Optics.

References and links

1. P.L. Kaufman, A. Alm, "Adler's Physiology of the Eye," Mosby (2003)
2. R. H. Webb, G. W. Hughes, O. Pomerantzeff "Flying spot TV ophthalmoscope," Appl. Opt. **19**, 2991-2997 (1980)
3. R. H. Webb, G. W. Hughes, F. C. Delori, "Confocal scanning laser ophthalmoscope," Appl. Opt. **26**, 1492 (1987)
4. W. J. Donnelly III, A. Roorda, "Optimal pupil size in the human eye for axial resolution," J. Opt. Soc. Am. A **20**, 2010-2015 (2003)
5. S. Marcos, S. A. Burns, P. M. Prieto, R. Navarro, B. Baraibar "Investigating sources of variability of monochromatic and transverse chromatic aberrations across the eye," Vision Res. **41**, 3861-3871 (2001)
6. H. Hofer, P. Artal, B. Singer, J. L. Aragón, D. R. Williams, "Dynamics of the eye's aberration," J. Opt. Soc. Am. A **18**, 497-506 (2001)
7. J. Liang, D. R. Williams, D. T. Miller, "Supernormal vision and high-resolution retinal imaging through adaptive optics," J. Opt. Soc. Am. A **14**, 2884-2892 (1997)

8. J. Carroll, M. Neitz, H. Hofer, J. Neitz, D. R. Williams, "Functional photoreceptor loss revealed with adaptive optics: An alternate cause of color blindness," *PNAS* **101**, 8461-8466 (2004)
9. A. Roorda, F. Romero-Borja, W. J. Donnelly III, H. Queener, T. J. Herbert, M. C. W. Campbell, "Adaptive optics scanning laser ophthalmoscope," *Opt. Express* **10**, 405-412 (2002), <http://www.opticsinfobase.org/abstract.cfm?URI=oe-10-9-405>.
10. D. Huang, E. A. Swanson, C. P. Lin, J. S. Schuman, W.G. Stinson, W. Chang, M. R. Hee, T. Flotte, K. Gregory, C. A. Puliafito and J. G Fujimoto "Optical coherence tomography," *Science* **254**, 1178-1181 (1991).
11. S. A. Al-Chalabi, B. Culshaw and D. E. N. Davies, "Partially coherent sources in interferometric sensors," First International Conference on Optical Fibre Sensors, (1983)
12. R. C. Youngquist, S. Carr and D. E. N. Davies, "Optical coherence-domain reflectometry: A new optical evaluation technique," *Opt. Lett.* **12**, 158-160 (1987)
13. M. Mujat, R. Chan, B. Cense, B. Park, C. Joo, T. Akkin, T. Chen, J. de Boer, "Retinal nerve fiber layer thickness map determined from optical coherence tomography images," *Opt. Express* **13**, 9480-9491 (2005), <http://www.opticsinfobase.org/abstract.cfm?URI=oe-13-23-9480>.
14. B. Hermann, E. J. Fernández, A. Unterhuber, H. Sattmann, A. F. Fercher, W. Drexler "Adaptive-optics ultrahigh-resolution optical coherence tomography," *Opt. Lett.* **29**, 2142-2144 (2004)
15. Y. Zhang, J. Rha, R. S. Jonnal, D. T. Miller "Adaptive optics parallel spectral domain optical coherence tomography for imaging the living retina," *Opt. Express* **13**, 4792-4811 (2005), <http://www.opticsinfobase.org/abstract.cfm?URI=oe-13-12-4792>.
16. R. Zawadzki, S. Jones, S. Olivier, M. Zhao, B. Bower, J. Izatt, S. Choi, S. Laut, and J. Werner, "Adaptive-optics optical coherence tomography for high-resolution and high-speed 3D retinal in vivo imaging," *Opt. Express* **13**, 8532-8546 (2005), <http://www.opticsinfobase.org/abstract.cfm?URI=oe-13-21-8532>.
17. A. Gh. Podoleanu, G. M. Dobre, D. J. Webb, D. A. Jackson, "Coherence imaging by use of a Newton rings sampling function," *Opt. Lett.* **21**, 1789-1971 (1996)
18. A. Gh. Podoleanu, G. M. Dobre, D. A. Jackson, "*En-face* coherence imaging using galvanometer scanner modulation," *Opt. Lett.* **23**, 147-149 (1998)
19. A. Gh. Podoleanu, J. A. Rogers, D. A. Jackson, "OCT *en-face* images from the retina with adjustable depth resolution in real time," *IEEE J. Sel. Top. in Quantum Electron.*, **5**, 1176-1184 (1999).
20. A. Gh. Podoleanu, D. A. Jackson, "Combined Optical Coherence Tomograph and Scanning Laser Ophthalmoscope," *Electron. Lett.* **34**, 1088-1090 (1998)
21. A. Gh. Podoleanu, G. M. Dobre, R. G. Cucu, R. Rosen, P. Garcia, J. Nieto, D. Will, R. Gentile, T. Muldoon, J. Walsh, L. A. Yannuzzi, Y. Fisher, D. Orlock, R. Weitz, J. A. Rogers, S. Dunne, A. Boxer, "Combined Multiplanar Optical Coherence Tomography and Confocal Scanning Ophthalmoscopy," *J. Biomed. Opt.* **9**, 86-93 (2004).
22. A. Gh. Podoleanu, D. A. Jackson, "Noise Analysis of a Combined Optical Coherence Tomograph and a Confocal Scanning Ophthalmoscope," *Appl. Opt.* **38**, 2116 - 2127 (1999)
23. The European Committee for Electrotechnical Standardization, "Safety of Laser Products" (2003)
24. A. Gh. Podoleanu, M. Seeger, G. M. Dobre, D. J. Webb, D. A. Jackson, "Transversal and longitudinal images from the retina of the living eye using low-coherence reflectometry," *J. Biomed. Opt.* **3**, 12-20 (1998)
25. F. Roddier, "Adaptive Optics in Astronomy," Cambridge University Press (1999)
26. E. Dalimier, C. Dainty, "Comparative analysis of deformable mirrors for ocular adaptive optics," *Opt. Express* **13**, 4275-4285 (2005), <http://www.opticsinfobase.org/abstract.cfm?URI=oe-13-11-4275>.

1. Introduction

The human retina is an extremely complex structure that is composed of six different types of neuron cells and ten histological layers within a depth of a few hundred microns [1]. Imaging the retina using techniques that produce high resolution images has opened novel diagnosis avenues. Here we present a novel combination of adaptive optics (AO) with simultaneous *en-face* optical coherence tomography (OCT)/scanning laser ophthalmoscopy (SLO) system for high resolution imaging of the *in-vivo* human retina.

SLO is a flying spot imaging technique based on confocal microscopy that is used to obtain high resolution retinal images of the *in-vivo* human eye [2, 3]. SLO uses scanning mirrors to sweep the probing beam over the retina and a pinhole that is placed in a plane conjugate to the depth of the retina that is being imaged. This pinhole blocks spurious light coming from scattering bodies that lie at other depths, providing in this way optical depth sectioning.

The achievable resolutions of an SLO system are typically of around 300 μm in depth and 10 μm lateral [4]. These values are mainly limited by the aberrations of the patient's eye, since the images are obtained through its optics. These aberrations vary widely between subjects [5],

and are not constant in time [6]. AO has been demonstrated as a suitable method to dynamically correct for these aberrations [7], improving the quality of the images obtained using several available retinal imaging techniques. These techniques allow, for example, the diagnosis of visual disorders involving cone loss, which is possible by means of an AO assisted fundus camera [8]. AO has also been combined with SLO systems, and results have been reported achieving 100 μm depth resolution and 2.5 μm lateral resolution [9].

OCT [10] is a technique based on low coherence interferometry [11, 12] that is able to reconstruct tomographic (sectional) images of the sample under study. It is usually implemented as a Michelson interferometer, in which the pattern of interference between the reference and object beams is used to determine the amount of light reflected back from a certain point within the volume of the sample under study. A broad band source is used for illumination, and therefore the two beams only produce an interference pattern when their optical paths differ by less than the coherence length of the source. This implies that the bandwidth of the source determines the depth resolution of the OCT system. Lateral resolution achieved using OCT for retinal imaging is comparable to that obtained using SLO, but depth resolution is significantly higher, since it can reach values of just a few microns depending on the bandwidth of the light source used. The high depth resolution of OCT images allowed the development of novel diagnosis methods, such as the follow-up of the nerve fiber layer thickness in glaucoma cases [13].

Similar to SLO, lateral resolution in OCT for retinal imaging is limited by the aberrations of the subject's eye and AO has also been used to improve its performance. An increase in the signal-to-noise ratio (SNR) of up to 9 dB was obtained when AO was applied in a single path configuration to a time domain OCT where an OKO mirror was used to correct for aberrations over a 3.6 mm diameter pupil [14]. The correction of ocular aberrations in this case, produced an increase on the value of the Strehl ratio from 0.04 to 0.46. An increase of 11.4 to 13.1 dB in the SNR has been reported in the case of a single path correction applied to a Fourier domain OCT using a Xinetics mirror and 6 mm diameter beam [15]. It is known that spectral domain OCT can provide better SNR than time domain OCT, which may explain the better results obtained, but also the difference in the equipment and design of the two systems mentioned may explain the difference in the results obtained. Similar enhancement in strength was reported using a double path AO correction configuration (it uses the deformable mirror in both beams going to and returning from the eye), [16] using a Fourier domain OCT.

However, all these reports refer to the traditional OCT sectioning, where B-scans were produced. Due to the use of fast axial scanning, the OCT images delivered lie in a plane parallel to the optical axis, i.e., they are oriented in a direction perpendicular to that of SLO images.

We developed flying spot *en-face* OCT, which allows generation of B-scans as well as OCT images with the same orientation as that of SLO images (C-scans) [17, 18]. In this technique scanning mirrors are used to move the focused probing beam over the surface of the sample to be imaged. The scanning configuration in *en-face* OCT is very similar to that used in SLO, with the fast scanning along the line in the C-scan raster.

Previous results [19] have shown that the higher the depth resolution, the more fragmented the *en-face* OCT image. This effect often makes it difficult for a visual scientist or ophthalmologist to determine the exact spatial location of the retinal patch imaged. Therefore, to help with the interpretation of the *en-face* OCT images, a dual imaging concept was suggested [20], where an SLO type image of coarser depth resolution is provided to guide the high depth resolution C-scan OCT image. The performance of such combined instrument was evaluated on several pathology cases [21]. Because the two images show pixel-to-pixel correspondence [22], the SLO image can be used to precisely guide the exploration in the OCT channel. Furthermore, specific orientation and location of B-scan slices can be guided by the information in the SLO image. We have also shown (a report is being prepared for publication) that small defects in

the retina can be missed when performing B-scan imaging only. Higher transverse resolution allowed by aberrations correction using AO will further enhance the quality of both *en-face* OCT and SLO images and hence this unique guiding capability. On the other hand, because OCT is based on interference, speckle noise is present, which sometimes obscures scattering features smaller than the speckle size in the retinal images. However, less speckle is present in SLO images when using low coherence sources. This demonstrates another advantage of the dual instrument, which synergetically benefits from the combination of information provided by the two images: low speckle noise in the SLO image, and high depth resolution in the OCT image.

In this article, a combined *en-face* OCT/SLO system for *in-vivo* retinal imaging is presented, equipped with an AO closed loop to correct for the ocular aberrations in both OCT and SLO channels.

2. System description

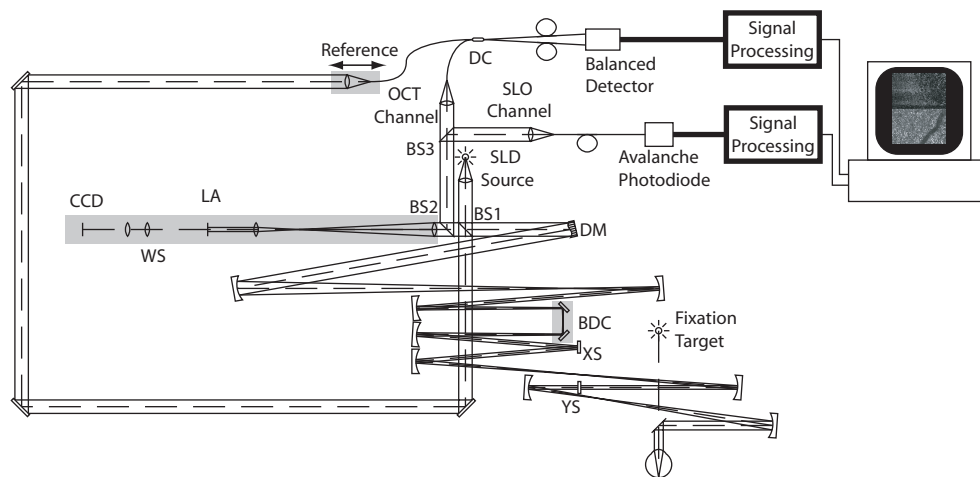


Fig. 1. AO-OCT/SLO system; SLD: Superluminescent diode; BS: beam splitter; DM: deformable mirror; BDC: Badal defocus corrector; XS: X scanner; YS: Y scanner; WS: wavefront sensor; LA: lenslet array; DC: directional coupler.

Figure 1 shows a schematic diagram of the AO-OCT/SLO system. A superluminescent diode (SLD) is used with central wavelength at 831 nm, and 17 nm bandwidth (which determines a depth resolution of approximately 13 μm in the eye). The source beam is collimated and then split by a beam splitter (90 %T / 10 %R, BS1 in Fig. 1) into the reference and probing beams. The probing beam is reflected by the deformable mirror (DM), and then sent via a Badal defocus corrector (BDC) and x or line (XS) and y or frame (YS) scanners to the subject's eye. The scanners are driven at 2 Hz (the frame scanner) and 700 Hz (the line scanner). A series of telescopes built using pairs of spherical mirrors are incorporated between these elements. Mirrors have been chosen rather than lenses to avoid the stray reflections from lens surfaces that may affect the performance of the wavefront sensor (WS). These telescopes conveniently alter the diameter of the beam in order to match the aperture of different elements in the probing path, and convey a probing beam of 6 mm in diameter through the subject's pupil plane. The telescopes also ensure that the subject's pupil plane is conjugate to the XS, YS and DM planes.

The system presented here uses a double pass configuration [16]. This and the use of large focal length mirrors determined a large size layout, and in consequence the object and reference

arms are quite long (the object arm is ~ 5 m in length one way). This may lead to thermal fluctuations of the optical path difference (OPD) and launching problems. Therefore an isolated optical bench was used.

The optical power reaching the cornea of the subject is $300 \mu\text{W}$, which is well below the $700 \mu\text{W}$ threshold dictated in [23] for a non-scanning beam at 831 nm in a configuration like the one presented in Fig. 1. Light scattered back from the patient's retina passes a second time through the object arm, and reaches a second beam splitter (1 % T / 99 % R BS2 in Fig.1). Light transmitted through BS2 is collected by the wavefront sensor (WS). This has been implemented as a Shack-Hartmann WS and is described with more detail in the following section.

Light reflected at BS2 reaches a third beam splitter (BS3 in Fig. 1), to divert 30% of the incoming beam to the SLO channel, and transmit the rest into the OCT channel. In both channels light is injected into single mode fibers. This ensures a high confocal parameter in both channels and good spatial rejection of multiple scattered light. The other end of the fiber in the SLO channel is connected to an avalanche photodiode. In the OCT channel, light is guided towards a single mode directional coupler (DC) where it interferes with that coming from the reference arm. Both output fibers from the DC are connected to two pin photodetectors in a Nirvana 2007 balanced photodetection unit.

The last focusing element and the fiber end in the reference arm are fixed on a translation stage that has a range of 2.5 cm, useful to allow coherence matching for different lengths of the volunteers eyes. The stage can also be used to construct B-scans images of the retina, which are obtained by stopping the frame scanner, and moving the translation stage along the optical axis of the reference beam [24]. Such B-scan images are similar to longitudinal scans of the retina delivered by traditional OCT, however, in this case, the fast direction of scanning is perpendicular to the optical axis, while the slow scanning is performed along the optical axis.

2.1. Adaptive optics system description

The AO system implemented consists of a Shack-Hartmann wavefront sensor based on an Andor Technologies CCD camera that works in closed-loop together with a 37 actuator membrane deformable mirror from Flexible Optics (OKO Technologies). Although such a sensitive CCD camera is not essential for an application like the one described in this paper, it has allowed lower light levels to be used since only 0.9% of the light scattered back from the subject's retina was used for wavefront sensing, maximizing the amount of light used in the imaging arms. However, in comparison with previous implementations where AO was combined only with either SLO or OCT, in our system, AO is combined with both OCT and SLO systems at the same time. Therefore, the weak signal backscattered from the eye is shared by the OCT and SLO channels and the WS. This justifies, in principle, the need for a better camera than those used in previous reports.

An array of square lenslets of $200 \mu\text{m}$ pitch is used in the WS. The lenslets are magnified so their pitch in the patient's pupil is $390 \mu\text{m}$. Thus, for a volunteer's pupil of 6 mm, 120 sub-apertures are used.

The system is able to measure and correct the subject's eye aberrations at a frame rate of 9 frames per second. This frame rate is limited by the exposure time of the CCD camera used in the WS. Since the images are obtained at a rate of 2 fps, the aberration is measured and corrected 4 times for each C-scan image obtained. The bandwidth of the AO system is approximately 1 Hz, estimated as suggested in [25].

3. Results

A chin rest and bite bar were used to stabilize the head of the subjects, but no drops to dilate the pupil or block accommodation were used. The AO-OCT/SLO system described above was

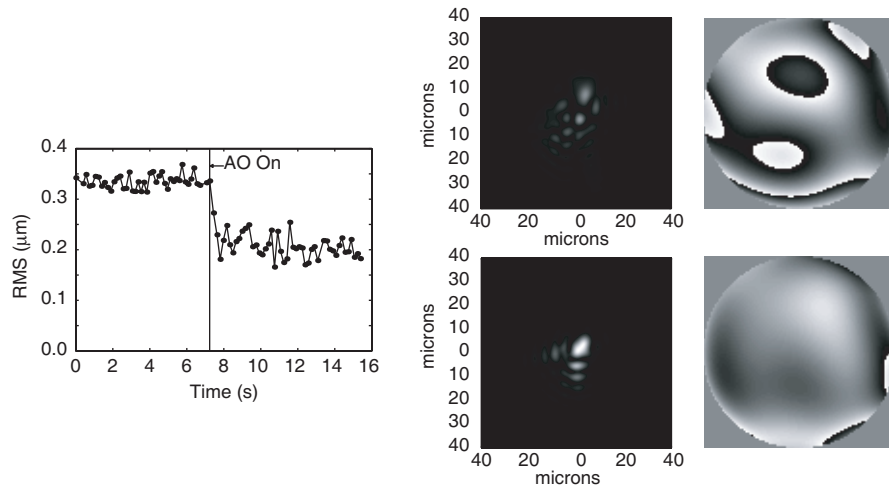


Fig. 2. The graph on the left shows the temporal evolution of the reconstructed RMS before and immediately after the AO closed-loop system is turned on. On the right, the PSF and reconstructed wavefront without adaptive optics correction (top) and with adaptive optics correction (bottom) are shown.

used to image the retina of two healthy volunteers, who did not require correction for defocus or astigmatism. The volunteers did not wear contact lenses or spectacles. The Badal was used to compensate for defocus. Every time the Badal was acted upon, the length of the reference path had to be modified to match the new path length in the object arm. The use of additional lenses to optimize defocus was dismissed, since the whole pupil was illuminated and if used, they would have produced disturbing reflections for the wavefront sensor.

The volunteer was guided by an operator to position his eye in the system in order to match the position of the spots in the WS with that of the spot pattern used as the reference frame. Also the tilting of the volunteer's head was optimized to inject the maximum light into the optical fiber. The Badal was adjusted subjectively, for maximum sharpness of the scanning line seen by the volunteer. This, we believe, resulted in placing the focus at the level of photoreceptor layer, and was confirmed by the SLO images, that correspond to the photoreceptor layer, as will be explained later. When these two steps were performed satisfactorily, the AO was turned on.

Figure 2 shows the evolution of the root mean square (RMS) values of the deviation of the wavefront from a plane surface. Information from the WS spot pattern was used to reconstruct the aberrated wavefront using a Zernike decomposition (ignoring the tilt components), and the RMS of the deviation of the wavefront from a plane surface over the pupil is shown for a period of time in which AO correction was applied. The figure shows how the system is able to reduce the reconstructed wavefront RMS to a value of around $0.2 \mu\text{m}$ for this particular eye (subject AB). This is in good agreement with previous reports using the same deformable mirror [26], and is consistent with the improvement in the lateral resolution observed, which will be detailed in the following section. A reconstructed wavefront aberration map is also shown in Fig. 2 along with the corresponding PSF for the same measurement without (top) and with (bottom) AO correction. An increase in the Strehl ratio has been measured, being 0.1 without and 0.2 with adaptive optics correction. Although this value is not close to that reported by Hermann *et al.* [14], it should be taken into account that our system is based on a double pass configuration, and the pupil size is larger in the case presented here (6 mm compared to 3.68 mm). Furthermore, in our system the number of subapertures used is more than double the number used in [14]. These

factors, along with the limited performance of the mirror used may explain the difference in the results obtained.

The effect of AO on the signal of both OCT and SLO channels has been characterized by using different parameters. First, an increase in the light intensity injected into both the OCT and SLO fiber optics is expected, since the beam is better focused and concentrated over a smaller area when adaptive correction is applied.

Due to the reduction of the wavefront aberration, an increase in the SNR is expected, as reported in [14, 15]. Such improvement has been observed in our system for both channels and both volunteers. Because the noise does not change when the AO loop is turned on, an increase in the signal strength due to AO produces a similar increase in the SNR. The SNR was improved by 4 to 6 dB on the OCT channel, and by 7 to 9 dB in the SLO channel. These values were measured for the two subjects a number of times. They were different for each subject, but repeatable for each of them. Because the OCT signal is proportional to the square root of the reflectivity, it is expected that the improvement in dB in the OCT channel to be only half of that in the SLO channel. The improvement in SNR measured for the OCT channel is lower than the values available in literature and in particular it is lower than that obtained with a similar deformable mirror [14], although the pupil size in that case, 3.7 mm, was significantly smaller than in the case presented here, 6 mm. Using a Xinetics mirror, 11 to 13 dB was reported in [12] for a similar pupil size as that we used.

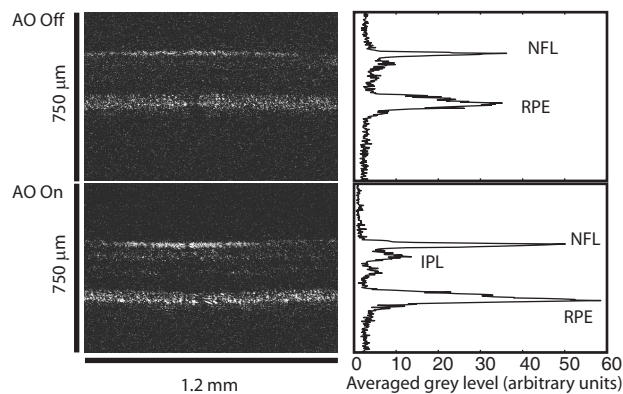


Fig. 3. Longitudinal OCT images obtained from the right eye of the volunteer (AB) before and after applying adaptive optics correction. The images are from a patch of the retina at 5 deg from the subject's fovea in the nasal direction. On the right, the average of the grey levels performed along the x axis shows an improvement in the signal strength due to correction.

Figure 3 shows two *en-face* B-scan OCT images to compare the amplitude of the signal obtained with and without correction applied. Average of the grey levels along the x axis are used as quantitative values for comparing the strength of signal from different retinal layers. The peaks corresponding to the nerve fiber layer (NFL) and to the retinal pigment epithelium (RPE) are higher when adaptive correction is applied. Other peaks too, corresponding to layers that were almost masked by noise become more visible in the bottom right plot. This is the case of the layer labelled as the inner plexiform layer (IPL). Although the quality of the images is lower compared to those obtained using other systems [14, 15], the images presented serve as a guiding tool, and not as a result in themselves. They help identify the layer from which the *en-face* OCT images are collected. B-scans provide information about the intensity of the retinal layers at different depths, and this information helps to identify them in the process of

acquisition of *en-face* images.

When AO is applied, there are two effects on the signal strength, increase due to aberrations compensation at the depth where the system is focused at and decrease of the signal for scattering points situated out of focus, due to the confocal profile narrowing. The theory says that the confocal profile under AO correction for a pupil of 6 mm should be less than the thickness of the retina. Therefore the signal should only increase at the depth where the focus is. The results presented show how the signal increases at all depths, although the increase is higher at the RPE (adjacent to the photoreceptor layer), where the system is actually focused. The layer at which the system is focused could be inferred from the SLO image, as it matches the structure corresponding to the photoreceptor layer shown in [9].

Since the OCT channel is focused at the same layer, this could explain the higher increase in the OCT signal at that depth when the AO correction is applied. As for the increase in the signal at other depths, this demonstrates that the signal strength enhancement due to aberration compensation exceeded the decrease due to the confocal profile narrowing on layers that were out of focus. This effect can also be observed in the images shown in [14], where an OCT system enhanced with AO is presented. Although its depth range should be smaller than the thickness of the retina, the quality of the image is improved at all the depths. We have not collected images with focus shifted towards the NFL. In fact, it was difficult to evaluate an improvement in the confocal profile of the OCT core, although we believe that some improvement took place. Therefore we have not studied the effect of focus change on the relative ratio of peaks in the OCT B-scan. This is dependent on the performance of the AO channel, whose behaviour was reported in previous AO-SLO reports, and is not typical for the *en-face* OCT/SLO configuration presented.

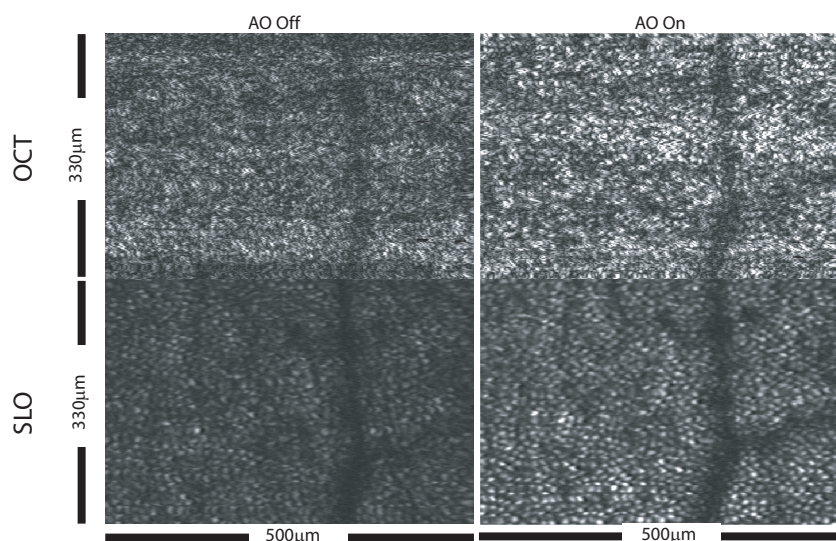


Fig. 4. *En-face* OCT and SLO images obtained from the same area of the DM's retina, before and after applying adaptive correction. The size of the retinal patch imaged is 330x500 μm , and the pixel size is 1x1 μm . The depth selected is at the photoreceptor level.

Figure 4 shows a pair of C-scan OCT and SLO images before and after adaptive correction was applied. They are taken at 5 deg from the fovea towards the nasal direction, and their size is $500 \times 330 \mu\text{m}$. For the lateral size of images in Fig. 4, this corresponds to 1 micron per electronic pixel.

An improvement in the transversal resolution of the *en-face* images was noticed. To evaluate this enhancement we calculated the power spectral density (PSD) of the images obtained from the OCT and SLO channels. We determined a circle of radius r for which the volume under the PSD curve was 99 % of the total volume under that curve. Using this criterion, an improvement in the resolution of the images has been detected, showing $r = 6.5 \mu\text{m}$ before and $5 \mu\text{m}$ after applying adaptive correction in both channels. This slight improvement in the transversal resolution together with the enhancement in the signal strength noticed leads to better observation of photoreceptor structure in both OCT and SLO images after the AO loop is switched on.

4. Conclusion

For the first time, a dual *en-face* OCT/SLO channel system has been presented that incorporates an AO loop to correct for the eye aberrations in both channels. The system can simultaneously acquire OCT C-scan images with high depth resolution and SLO images with low speckle noise. These images present pixel-to-pixel correspondence. It can also produce B-scan *en-face* OCT images only by changing the operation mode. The two transverse scanners have been separated in order to keep the aberrations in the interface optics of the probing beam low, and the interface optics was equipped with spherical gold coated mirrors to avoid reflections from lenses. Such a system is ideally suited for further improvements in the AO technology applied to the eye. The correction achieved in the present system is mainly limited by the parameters of the deformable mirror used and a comparative study of commercially available low-cost deformable mirrors [26] predicts that other mirror technologies will yield greatly improved performance. If confocal profiles as narrow as tens of microns are achievable by using better components, then dynamic focus is required in the OCT channel which would render the A-scan based OCT technology inefficient. The *en-face* OCT is ideally suited to dynamic focus, although not implemented here. For the system presented, the rate of focus adjustment required is 2 Hz, which could easily be achieved mechanically for both B and C-scan regimes of operation. Although we obtained moderate improvements by applying the AO, we illustrated the basic functionality of such a novel system in both regimes of operations, B and C-scan, and reported improvement in the performance of the OCT and SLO channels when the AO was switched on, with images from two volunteers. In addition to enhancement in the strength of the signal, we have also noticed a slight improvement in the transverse resolution in both channels when the AO was turned on. The images obtained allowed identification of individual cells in the OCT channel at the photoreceptor level. Because there is pixel-to-pixel correspondence between OCT and SLO images obtained, the lateral improvement in resolution is valid for both channels to the same extent. Other layers have been visualized comparatively in the B-scan longitudinal images obtained with the same system. Further work is required in order to focus the beam accurately on different retinal layers and improve the level of correction to obtain full benefit of the *en-face* OCT imaging technology. The system represents a step forward towards imaging with high resolution the different layers and the cells in the *in-vivo* human retina.

Acknowledgments

A. Podoleanu and A. Bradu acknowledge EPSRC support, grant GR/S18120/01. A. Podoleanu further acknowledges the Leverhulme Trust for a research fellowship. C. Dainty and D. Merino acknowledge support from the Science Foundation Ireland under Grant 01/PI.2/B039C. The authors thank Ophthalmic Technology Inc, Toronto, Canada for the frame grabber.